Shahid Beheshti University

Sustainable Earth Trends

Journal homepage: http://sustainearth.sbu.ac.ir

Photocatalytic degradation of organic pollutants in aqueous solutions using noble metal-based nanocomposites

Maryam MozafarJalali[a], Mahmood Hajiani[b*], Mohammad Hossein Sayadi[c]

[a] Department of Environmental Engineering, Faculty of Natural Resources and Environment, University of Birjand, Birjand, Iran
[b] Department of Civil Engineering, Faculty of Engineering, University of Birjand, Birjand, Iran
[c] Iranian National Institute for Oceanography and Atmospheric Science (INIOAS), Tehran 1411813389, Iran

ABSTRACT

Magnetic noble metal nanoparticles have garnered considerable attention in recent decades for removing organic pollutants, owing to their exceptional photocatalytic activity, reusability, chemical stability, and environmental compatibility. This study investigates the photocatalytic degradation efficiency of dyes, serving as representative organic pollutants, using Fe_2O_3/Bi/GO nanocomposite under UV light. The Fe_2O_3/Bi/GO nanocomposite was synthesized via a hydrothermal method, and its structure, morphology, and other properties were characterized using XRD, FE-SEM, and VSM techniques. The characterization results confirmed the successful synthesis of the Fe_2O_3/Bi/GO nanocomposite, with particle sizes ranging from 30 to 60 nm and notable magnetic properties. Key factors influencing dye removal, including pH, catalyst concentration, and initial dye concentration, were systematically evaluated. The findings revealed that the Fe_2O_3/Bi/GO nanocomposite exhibits excellent photocatalytic activity for removing dyes from textile wastewater. The optimal pH for degrading Yellow 3G was 3, while for Methylene Blue, it was 11. The ideal catalyst dosage for both dyes was determined to be 0.3 g/L. Under these conditions, 98.23% of 30 mg/L Yellow 3G and 96.87% of 20 mg/L Methylene Blue were effectively photodegraded. Furthermore, the synthesized nanocomposite demonstrated strong recyclability, retaining its performance over five consecutive cycles. With its high efficiency and stability, this photocatalyst offers a practical, sustainable, and eco-friendly solution for removing organic pollutants from water sources.

ARTICLE INFO

Keywords:
Dye
Emerging pollutants
Photocatalysis
Wastewater treatment

Article history:
Received: 30 November 2024
Accepted: 04 January 2025

*Corresponding author
E-mail address:
hajiani@birjand.ac.ir
(M. Hajiani)

Citation:
MozafarJalali, M. et al., (2026). Photocatalytic degradation of organic pollutants in aqueous solutions using noble metal-based nanocomposites, *Sustainable Earth Trends:* 6(2), (51-61).

DOI: 10.48308/set.2025.238150.1102

1. Introduction

One of the fundamental environmental challenges is the declining quality and availability of water resources (Sayadi and Heshmatpour, 2024). With population growth and increasing industrialization, the contamination of water sources by industrial pollutants has emerged as a significant threat to public health (Sayadi et al., 2022). Among these pollutants, organic compounds such as dyes represent a major concern for aquatic environments (Poorsajadi et al., 2021). The extensive use of dyes across various industries—including textiles, resins, papermaking, plastics, and cosmetics—has led to the release of colored effluents into the environment (Guo et al., 2022). The overconsumption of dyes and their infiltration into environmental systems have numerous adverse effects on the quality of soil, surface water, groundwater, municipal wastewater, and even drinking water supplies (Lotfi et al., 2024). Due to their high environmental stability and low biodegradability, most dyes persist in the environment for extended periods. Even at low concentrations, dye compounds inhibit photosynthesis by blocking light penetration in aquatic ecosystems (Lotfi et al., 2024; Sayadi and Heshmatpour, 2024).

Additionally, because of their resistance to biodegradation, dyes are not metabolized in living organisms, leading to their accumulation in the human body and other organisms. This buildup of toxic substances is associated with various health risks, including mutations, cancers, allergies, skin irritations, and heart diseases (Mozafarjalali et al., 2020; Khosravi Mohammad Soltan et al., 2021). Given the harmful environmental impacts of dyes, it is crucial to treat dye-containing wastewater before its release into the environment. To date, various methods such as adsorption, coagulation, biological treatments, and membrane filtration have been developed for dye removal. However, each of these approaches faces limitations and challenges that reduce their effectiveness in eliminating dye residues from industrial wastewater (Sayadi et al., 2022). Many of these conventional methods are time-consuming, expensive, and fail to fully decompose organic pollutants, merely transferring them from one phase to another (Hajiani et al., 2023). To overcome these limitations, advanced oxidation processes (AOPs) have been developed. AOPs degrade pollutants through reactive radicals generated by chemical oxidants, such as ozone and hydrogen peroxide, often in combination with auxiliary energy sources like ultraviolet radiation, electric current, gamma rays, or ultrasound (Wang et al., 2023). Among AOPs, photocatalytic processes have gained attention due to their high efficiency, ease of operation, low energy consumption, mild reaction conditions, and lack of secondary pollutant formation (Kumari et al., 2023; Ahmadpour et al., 2024). These processes are highly effective in breaking down both organic and inorganic pollutants (Lanjwani et al., 2024), converting them into simple, low-risk molecules, and ultimately achieving complete mineralization and pollutant removal. A critical factor in the efficiency of photocatalysis is the selection of a highly effective photocatalyst. Fe_2O_3, a magnetic material with a narrow band gap (2.1 eV), has been extensively studied due to its advantages, including low cost, excellent photocatalytic activity under visible light, chemical stability, non-toxicity, magnetic properties, and reusability (Shah, 2023). However, the use of Fe_2O_3 alone is limited by the rapid recombination of electron-hole pairs generated during the photocatalytic process, which significantly reduces its overall effectiveness (Huang-Mu et al., 2023). To address this issue, numerous studies have explored the combination of Fe_2O_3 with other materials, such as noble metals, to create more effective photocatalysts (Devi et al., 2023). Bismuth-based photocatalysts have garnered increasing attention due to their high stability, resistance in both acidic and alkaline environments, and strong photocatalytic activity. Their unique structural and electronic properties further enhance their appeal (Naffeti et al., 2023). Additionally, bismuth-based compounds are widely used in photocatalytic applications due to their favorable energy band alignment, low toxicity, and cost-effectiveness (Roozbahani et al., 2024). On the other hand, graphene, a novel carbon nanomaterial, has been investigated for its ability to enhance the photocatalytic activity of nanocomposites, owing to its excellent electrical and thermal conductivity, low density, charge carrier mobility, mechanical strength, and high optical conductivity (Campos-Delgado and Mendoza, 2023). This study aims to synthesize an Fe_2O_3/Bi/GO nanocomposite and evaluate its effectiveness in the photocatalytic removal of both anionic and cationic dyes from aqueous solutions.

2. Material and methods

2.1. Chemicals

In this study, various materials were utilized for the synthesis of the nanocomposite and the execution of photocatalytic experiments. These materials included $FeCl_3 \cdot 6H_2O$ (99% purity), $FeSO_4 \cdot 7H_2O$ (99% purity), and bismuth nitrate ($Bi(NO_3)_3$) obtained from Merck (Germany), as well as graphene oxide (GO) sourced from Sigma Aldrich (USA). Methylene blue and Yellow 3G dyes were also procured from Merck (Germany). To adjust the pH of the solutions, sodium hydroxide (NaOH, 96% purity) and hydrochloric acid (HCl, 97% purity) from Merck (Germany) were employed. Deionized water was used for solution preparation at all stages of the experiments.

2.2. Synthesis of the (Fe_2O_3) nanoparticles

An aqueous solution of iron sulfate ($FeSO_4 \cdot 7H_2O$) and iron chloride ($FeCl_3 \cdot 6H_2O$) was prepared in a molar ratio of 1:2. A 1 M

sodium hydroxide (NaOH) solution, acting as a precipitating agent, was then added to the mixture until the pH reached 12. The solution was heated on a magnetic stirrer for one hour, with the reaction deemed complete when the color changed from light brown to dark brown. Finally, the resulting Fe_2O_3 nanoparticles were separated using a strong external magnet, washed with distilled water and ethanol, and dried in a vacuum oven at 70°C for one hour (Singh et al., 2023).

2.3. Synthesis of the (Fe_2O_3/Bi) nanocomposite

In this step, 100 mL of a $Bi(NO_3)_3 \cdot 5H_2O$ solution (50 mg/L) and 50 mL of methanol were added to the iron oxide nanoparticles (Fe_2O_3) synthesized in the previous step. The mixture was then stirred at room temperature for 30 minutes (Munir et al., 2024).

2.4. Synthesis of the (Fe_2O_3/Bi/GO) nanocomposite

Finally, 50 mL of a sonicated graphene oxide (GO) solution (20 mg/L) was added to the previous mixture, and the resulting solution was stirred for an additional 90 minutes. The obtained product was washed three times with distilled water and then dried at 80°C (Sun et al., 2017).

2.5. Characterization of the (Fe_2O_3/Bi/GO) nanocomposite

To identify and characterize the synthesized nanocomposite, several analytical techniques were employed, including Field Emission Scanning Electron Microscopy (FE-SEM), X-ray Diffraction (XRD), and Vibrating Sample Magnetometer (VSM) analyses. The crystal structure of the samples was determined using a Rigaku MiniFlex 600 XRD equipped with Cu Kα radiation (λ = 0.15418 nm). The morphology and structure of the nanocomposite were analyzed using a TE-SCAN MIRA3 FESEM. The magnetic properties of the composite were assessed with a Lake Shore 7403 VSM (Westerville, OH, USA). The pH of the solutions was measured using a composite glass electrode connected to a standard PHM 210 pH meter (Copenhagen, Denmark). Additionally, the concentration of the dye solution was measured using a Bio Spec-1601 spectrophotometer.

2.6. Photocatalytic experiments

The photocatalytic experiments for dye removal were conducted in a batch mode, considering various parameters including pH, contact time, catalyst dosage, and initial dye concentration. To evaluate the degradation efficiency of methylene blue and Yellow 3G pollutants and to determine the optimal values for pH, catalyst concentration, and dye concentration, a 200 mL batch reactor was utilized. A 6 W UV-C lamp was positioned in the center of the reactor, enclosed within a quartz cover to prevent direct contact with the solution. The reactor was wrapped in aluminum foil to enhance efficiency and strengthen light intensity while blocking the transmission of light to and from the reactor. Additionally, an aeration pump was employed to continuously mix the nanocatalyst within the solution. The pH of the solutions was adjusted using 0.01 M hydrochloric acid (HCl) and sodium hydroxide (NaOH). Various pH values (3, 5, 7, 9, and 11), photocatalyst dosages (0.1, 0.2, 0.3, 0.4, and 0.5 g/L), initial dye concentrations (10, 20, 30, 40, ad 50 mg/L), and contact times (5, 15, 30, 45, 60, and 90 minutes) were investigated and optimized. The experimental design was based on One Factor at a Time. Firstly, the optimal value of pH was measured. Then the pH of the solution was kept on optimum pH and the best catalyst dosage was determined. Finally, based on optimal values of pH and catalyst amount, optimum value of initial dye concentration was calculated.

Before activating the lamp and exposing the solution to light, the solution was stirred for 30 minutes in the dark to ensure equilibrium between the absorption and desorption processes of the photocatalyst and the pollutants. Once the stirring was complete, the light was turned on to initiate photocatalysis. At specified time intervals, a 5 mL sample was taken from the reaction solution and centrifuged at 4000 rpm for 15 minutes to separate the catalyst. Finally, the concentration of the remaining dye in the solution was measured using a UV-Vis spectrophotometer (Bio Spec-1601) at 404 nm for Yellow 3G and 660 nm for methylene blue. The removal efficiency of the pollutants was calculated using the following Eq. 1 (Li et al., 2018):

$$R(\%) = \frac{C_0 - C_t}{C_0} \quad (1)$$

Where R represents the percentage of dye removal, C_0 is the initial concentration of the

dye (mg/L), and C_t is the dye concentration at a specific time.

3. Results and discussion

3.1. Structural and morphological characteristics of nanocomposite (Fe_2O_3/Bi/GO)

FE-SEM was employed to examine the structure of the synthesized nanocomposite (Fig. 1). According to Fig. 1, graphene nanoplates are visible, along with nanoparticles exhibiting irregular and quasi-spherical morphology, which are composed of iron oxide and bismuth. The sizes of some of these particles are indicated in the figure. To assess the size distribution of the particles in the examined sample, 100 particles from the FE-SEM images for each sample were measured using ImageJ image processing software. The resulting particle size distribution histogram is presented in Fig. 2.

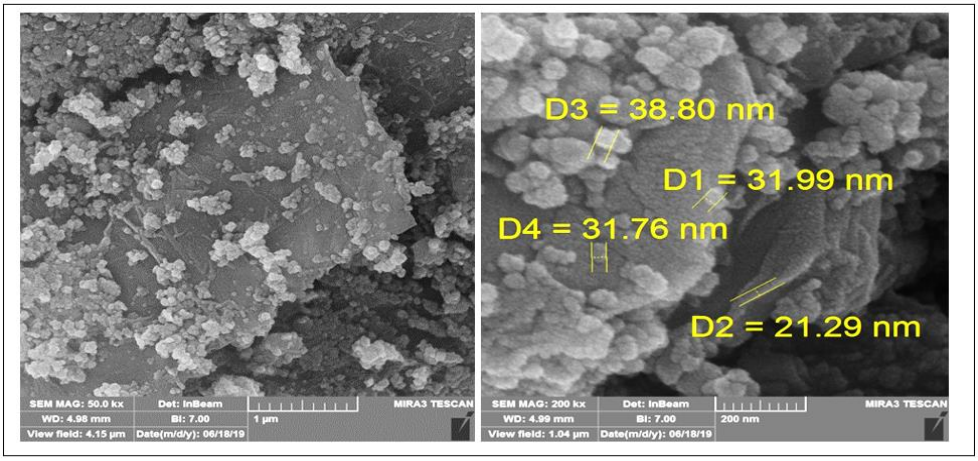

Fig. 1. FE-SEM of the synthesized photocatalyst of Fe_2O_3/Bi/GO.

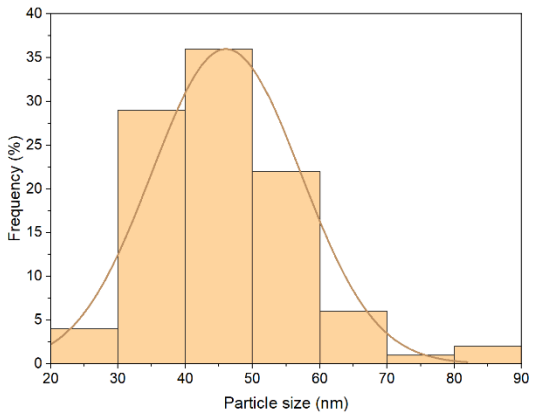

Fig. 2. Histogram of particle size distribution of the Fe_2O_3/Bi/GO.

In this histogram, the horizontal axis represents particle size, while the vertical axis indicates the number of particles within each size range, as measured by the software. According to the histogram presented in Fig. 2, of the 100 particles measured in the examined sample, 85% had dimensions ranging from 30 to 60 nm, with the largest proportion of nanoparticles falling within the 40 to 50 nm size range. The average size of the measured particles was calculated to be 46.08 ± 11.05 nm. Additionally, the largest particle measured was approximately 83 nm, confirming that all particles have diameters of less than 100 nm and thus qualify as nanoparticles (Munir et al., 2024).

3.2. Crystallinity of nanocomposite (Fe_2O_3/Bi/GO)

X-ray Diffraction (XRD) analysis is a widely used technique for identifying compounds and phases in nanomaterials. XRD enables the investigation of crystal structure, crystal size, interatomic distances, lattice parameters, and crystal defects (Chauhan and Chauhan, 2014). To examine the crystal structure of the synthesized catalyst, an XRD analysis was conducted, and the resulting diffraction pattern is presented in Fig. 3. The pattern reveals the presence of three distinct crystal phases: (1) a magnetite phase corresponding to reference code No. 96-900-5842, with a chemical formula of Fe_2O_3 and a cubic crystal structure; (2) a bismuth oxide phase corresponding to reference code No. 96-433-2560, with a chemical formula of Bi_2O_3 and an orthorhombic crystal structure; and (3) a graphene phase corresponding to JCPDS reference code No. 00-041-1487, with a chemical formula of C and a hexagonal crystal structure.

Thus, the presence of graphene phases alongside iron oxide and bismuth in the investigated sample is confirmed. The Miller indices for each peak are indicated on the corresponding peaks in Fig. 3. To find the size of the crystal, the Scherrer's equation relation is used (Hajipour et al., 2021):

$$D = K\lambda / (FWHM) \times \cos(\theta) \qquad (2)$$

Where D represents the crystal size, K is the shape factor, λ is the wavelength of the X-ray used, *FWHM* is the full width at half maximum, and θ indicates the peak position. Utilizing the values of *cos (θ)* and *FWHM*, along with the fixed values of λ and K, the crystal size can be calculated according to Scherrer's equation. The calculated crystal sizes are approximately 22.4 nm for the iron oxide phase and 29.4 nm for the bismuth oxide phase.

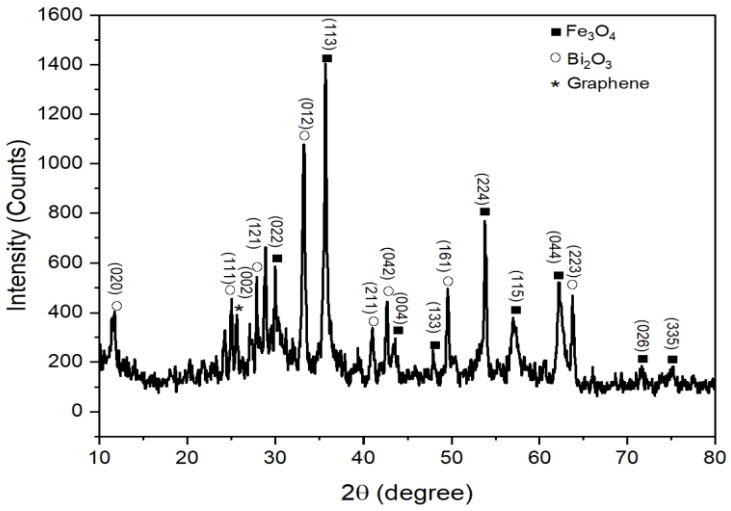

Fig. 3. XRD diffraction pattern of Fe_2O_3/Bi/GO.

To find the size of the crystal, the Scherrer's equation relation is used (Hajipour et al., 2021) (Eq. 2):

$$D = K\lambda / (FWHM) \times \cos(\theta) \qquad (2)$$

Where D represents the crystal size, K is the shape factor, λ is the wavelength of the X-ray used, *FWHM* is the full width at half maximum, and θ indicates the peak position. Utilizing the values of *cos (θ)* and *FWHM*, along with the fixed values of λ and K, the crystal size can be calculated according to Scherrer's equation. The calculated crystal sizes are approximately 22.4 nm for the iron oxide phase and 29.4 nm for the bismuth oxide phase.

3.3. Magnetic properties of nanocomposite (Fe_2O_3/Bi/GO)

The results of the Vibrating Sample Magnetometer (VSM) analysis, conducted to investigate the magnetic properties of the examined samples, are presented in Fig. 4.

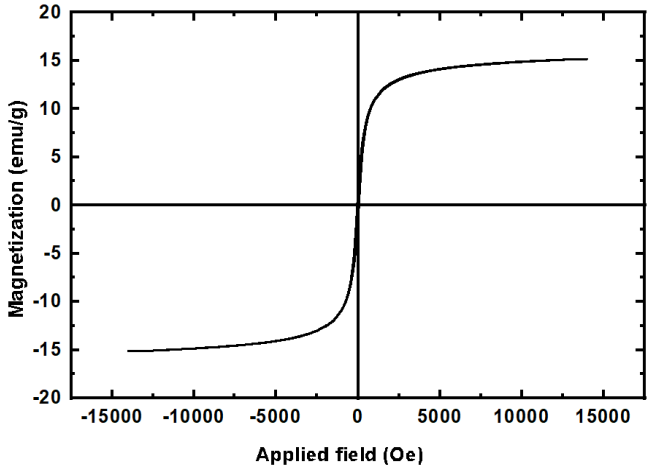

Fig. 4. VSM curve of the photocatalyst.

According to Fig. 4, the saturation magnetization value for the synthesized catalyst was 15.16 emu/g, indicating the significant magnetization capability of the nanocomposite. This strength is attributed to the presence of magnetite nanoparticles within the composite. The shape of the VSM curves, characterized by a very narrow hysteresis loop, suggests that the investigated sample exhibits superparamagnetic properties, which are typically observed in very small ferromagnetic or ferrimagnetic nanoparticles. The magnetic permeability of the material is notably high, allowing it to become quickly and strongly magnetized under an applied external field, while rapidly losing its magnetic properties once the field is removed (Nejati and Zabihi, 2012; Daoush, 2017).

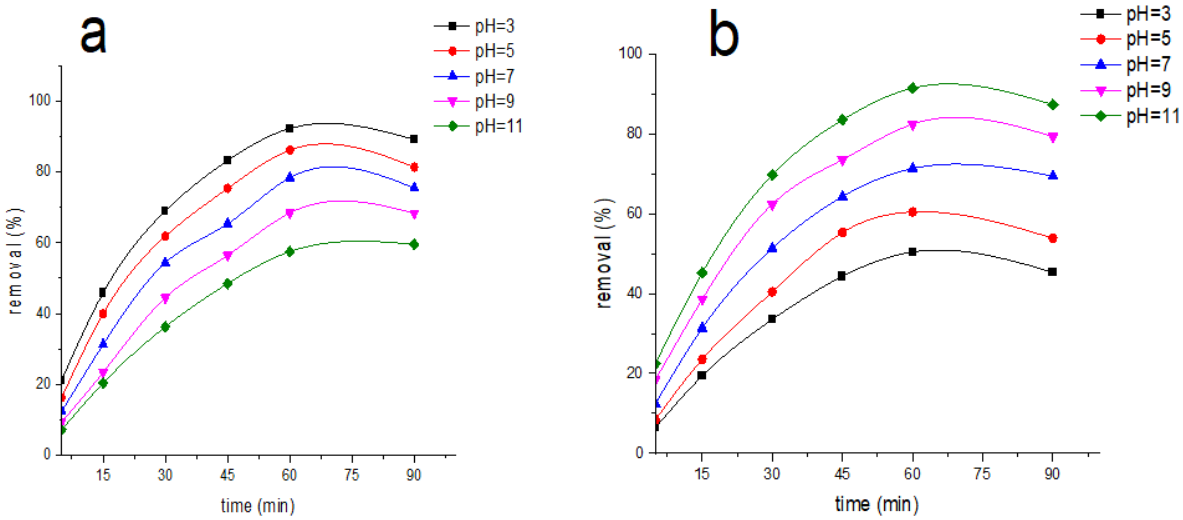

Fig. 5. Effects of pH on the removal of (a) yellow 3G, (b) methylene blue (initial dye concentration 20 mg/L and photocatalyst dosage 0.2 g/L).

3.4. Effect of pH

The pH of the environment is a critical parameter influencing the efficiency of the photocatalytic process. It affects the surface charge characteristics of the photocatalyst, which in turn impacts the adsorption and desorption capacity of organic compounds, as well as the ionization state of the catalyst surface (Rafiq et al., 2021). The effects of different pH levels (3, 5, 7, 9, and 11) on the performance of Fe_2O_3/Bi/GO in the photodegradation of Yellow 3G and methylene blue were investigated. The experimental conditions included an initial dye concentration of 20 mg/L and a synthesized nanocomposite dosage of 0.2 g/L. To adjust the pH, 0.01 M NaOH and HCl solutions were employed. The solution was stirred in the dark for 30 minutes to ensure the absorption-desorption balance between the photocatalyst and the dye before the UVC light was turned on. Fig. 5(a) illustrates the removal percentage of Yellow 3G, while Fig. 5(b) presents the removal percentage of methylene blue at various specific time intervals and different pH levels. As observed, the highest removal efficiency for Yellow 3G was recorded at 60 minutes with a pH of 3. It is evident that increasing the pH leads to a decrease in the removal of Yellow 3G. The enhanced removal efficiency of the anionic dye Yellow 3G in acidic conditions can be attributed to the positive surface charge of the catalyst in such environments, which facilitates the removal of dyes possessing a negative surface charge (Verma et al., 2021). At acidic pH, the presence of H^+ ions result in a positively charged catalyst surface. Given that Yellow 3G is an anionic dye with a negative charge, this electrostatic attraction enhances its removal efficiency (Tichapondwa et al., 2020). Conversely, in alkaline conditions, the presence of negatively charged hydroxide ions (OH^-) increases the number of negative active sites on the catalyst. Since Yellow 3G also carries a negative charge, this leads to electrostatic repulsion, ultimately reducing the efficiency of color removal (Ali et al., 2020). In acidic pH conditions, the high concentration of H^+ ions facilitate the generation of active hydroxyl radicals (OH).

These radicals possess strong oxidizing properties, significantly enhancing the removal of organic pollutants (Singh et al., 2024). Furthermore, in acidic environments, the recombination of electron-hole pairs is minimized, which is a crucial factor for the advanced degradation of organic pollutants (Tuama et al., 2024).

Fig. 5(b) illustrates the effect of pH on the degradation of methylene blue over time. As observed, increasing the pH leads to an enhancement in dye removal, with the highest removal efficiency recorded at pH 11. In alkaline conditions, the presence of hydroxide ions (OH^-) imparts a negative charge to the catalyst surface. Given that methylene blue is a cationic dye, it preferentially adsorbs onto negatively charged surfaces. Consequently, the increase in pH results in a higher density of negatively charged active sites on the catalyst, facilitating more effective degradation methylene blue (Chang et al., 2024).

3.5. Effect of initial dye concentration

The initial concentration of the dye in the solution significantly influences the removal efficiency, as a specific amount of catalyst can effectively react with a limited concentration of pollutant (Shaikh et al., 2023). Fig. 6 illustrates the effect of initial dye concentration on the efficiency of photocatalytic degradation over time. Various initial concentrations (10, 20, 30, 40, and 50 mg/L) were examined. As shown in Fig. 6, during the first 30 minutes of the reaction, the removal rates for both dyes were significantly high. Subsequently, while the removal rate slightly decreased, photodegradation continued to increase until the 60-minutes. After 60 minutes, the reaction reaches equilibrium, leading to a decrease in dye removal as even a small amount of dye adsorbed on the surface of the catalyst can desorb. During the first 30 minutes, the ratio of dye molecules to the active sites on the catalyst surface is relatively low, allowing greater accessibility to free sites. However, as time progresses and the active sites on the catalyst become saturated, the rate of dye removal begins to decline. Thus, the optimal duration for achieving the highest removal percentage of both pollutants is 60 minutes. As illustrated in Fig. 6(a), the removal efficiency of Yellow 3G increases with dye concentrations ranging from 10 to 30 mg/L. Similarly, for methylene blue, the removal efficiency improves with concentrations from 10 to 20 mg/L, as shown in Fig. 6(b). However, as the initial dye concentration increases further, the removal efficiency declines. This reduction in photodegradation at higher dye concentrations can be attributed to the repulsive forces between dye molecules, both in solution and on the catalyst surface (Lanjwani et al., 2023). Another reason for the decrease in photocatalytic degradation of dyes at higher concentrations is that an increase in dye concentration results in a greater number of organic substances being adsorbed onto the surface of the nanocatalyst. This leads to a reduction in available active sites for the absorption of hydroxyl ions, subsequently decreasing the production of hydroxyl radicals. Additionally, as the dye concentration rises, the penetration of photons to the surface of the nanocatalyst is hindered, resulting in diminished photon absorption by the nanocatalyst (Xu et al., 2023). Consequently, this reduction in photon absorption adversely affects the photocatalytic degradation efficiency of the dye (Kalaycıoğlu et al., 2023).

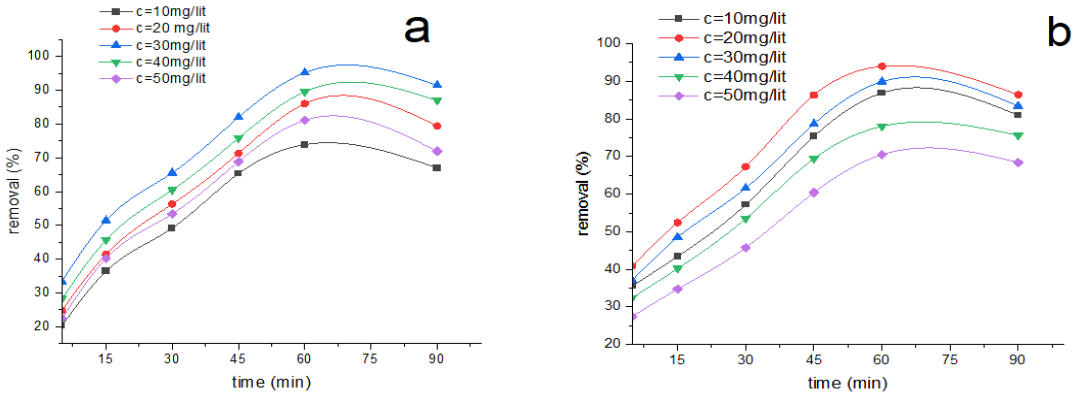

Fig. 6. The effect of initial dye concentration on the removal, (a) yellow 3G (pH 3 and photocatalyst dosage 0.2 g/L), (b) methylene blue (pH 11 and photocatalyst dosage 0.2 g/L).

3.6. Effect of photocatalyst dosage

Fig. 7 illustrates the effect of varying catalyst dosages (0.1, 0.2, 0.3, 0.4, and 0.5 g/L) on dye removal efficiency. An increase in catalyst dosage up to 0.3 g/L enhances the removal rate, achieving the highest photodegradation rates of 98.23% for Yellow 3G dye and 96.87% for methylene blue. However, further increasing the catalyst concentration to 0.5 g/L results in a decrease in removal efficiency.

A specific amount of catalyst provides a finite number of active sites for the adsorption of dye molecules, indicating that the catalyst dosage significantly influences dye absorption (Akbari et al., 2023). When the initial dye concentration is held constant, an increase in catalyst dosage creates a larger surface area and more accessible active sites, thereby enhancing the adsorption of dye molecules on the catalyst surface (Foroughipour and Nezamzadeh-Ejhieh, 2023). Additionally, higher catalyst dosages result in an increased number of free electrons in the conduction band and holes in the valence band, further improving dye removal efficiency (Abbood et al., 2023).

Nevertheless, beyond a certain catalyst dosage, particle aggregation and clumping can occur, leading to a decrease in the surface-to-volume ratio and, consequently, a reduction in dye removal efficiency. Furthermore, increasing the amount of catalyst can cause solution turbidity, which hinders light penetration and reduces degradation efficiency (Shabil Sha et al., 2024).

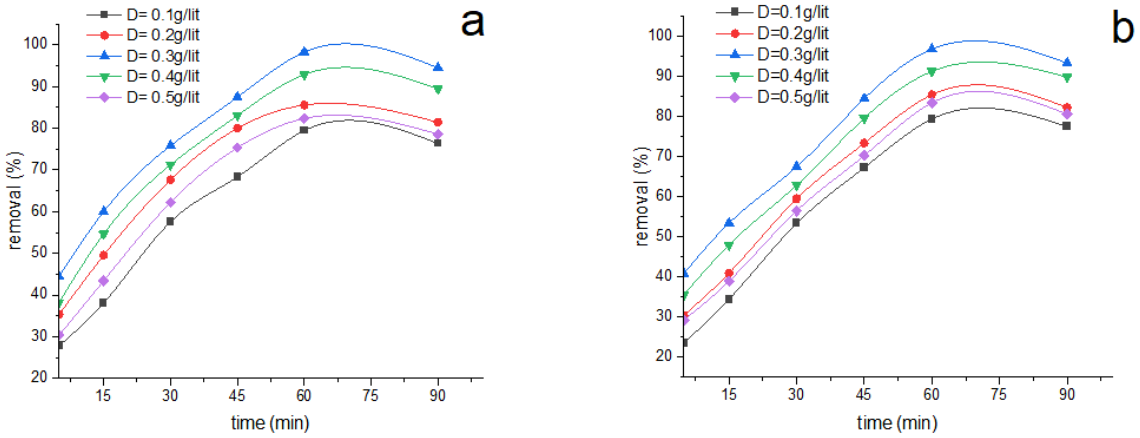

Fig. 7. Effect of catalyst dosage on removal, (a) yellow 3G removal (pH 3 and initial day concentration 30 mg/L), (b) methylene blue (pH 11 and initial day concentration 20 mg/L).

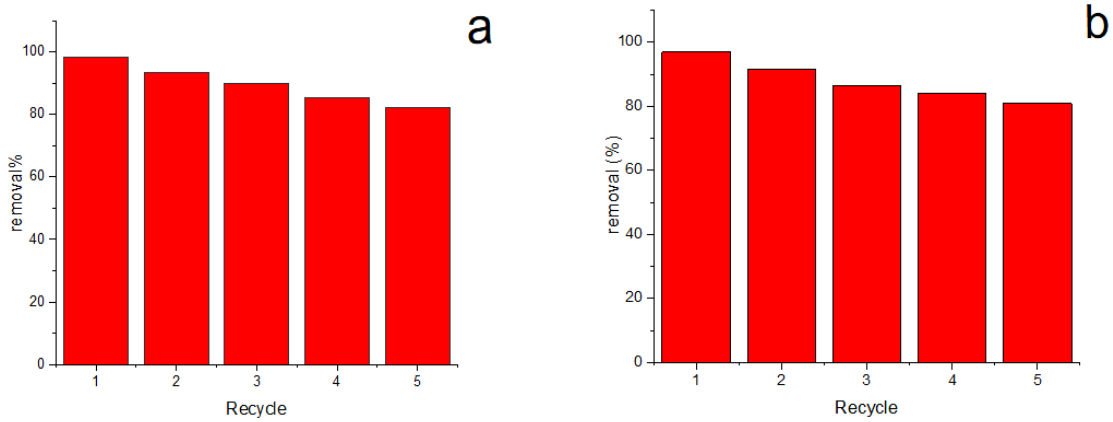

Fig. 8. Reusability of (Fe_2O_3/Bi/GO) after five cycles of photodegradation of (a) yellow 3G, (b) methylene blue.

3.8. Stability and reuse of Fe_2O_3/Bi/GO

Catalyst recovery and reuse are essential features, not only for ensuring chemical stability but also for economic viability. Consequently, enhanced stability and reusability of catalysts are significant advantages in the photocatalytic degradation of pollutants (Khorasanipour et al., 2023).

The stability of the nanocomposite (Fe_2O_3/Bi/GO) was evaluated for the photocatalytic degradation of methylene blue and Yellow 3G dyes under UV light. After each photocatalytic cycle, the used photocatalyst was recovered. Prior to reuse in the subsequent cycle, the catalyst was thoroughly washed several times with distilled water and ethanol, dried at 70°C for 8 hours, and then employed again for photocatalytic dye removal. Fig. 8(a) and (b) present the results of the nanocomposite recovery for the removal of Yellow 3G and methylene blue, respectively. As illustrated in Figure 8, the photocatalytic removal efficiency of the nanocomposite (Fe_2O_3/Bi/GO) remains nearly unchanged after five cycles of reuse. This indicates that the synthesized catalyst exhibits high stability and reusability, with only a slight decrease in photocatalytic removal efficiency. Specifically, the removal efficiency for Yellow 3G decreased from 98.23 to 82.25% (Fig. 8(a)), while the removal efficiency for methylene blue decreased from 96.87 to 80.86% after the fifth cycle (Fig. 8(b)). Given the strong magnetic properties of this nanocomposite and its reusability over successive cycles, this catalyst can be considered an efficient and cost-effective option for the removal of organic pollutants.

4. Conclusion

Conventional wastewater treatment methods often fail to effectively address dye-contaminated wastewater; however, advanced oxidation processes like photocatalysis have shown significant potential for degrading emerging organic pollutants. In this study, an Fe_2O_3/Bi/GO nanocomposite photocatalyst was successfully synthesized and characterized using FE-SEM, XRD, and VSM analyses. The nanoparticles exhibited an average size of 46.08 ± 11.05 nm and demonstrated notable magnetic properties. To assess the photocatalyst's efficiency in dye degradation, two dyes—one cationic and one anionic—were selected and treated in a 200 mL batch reactor under UVC light. The influence of various parameters, including pH, catalyst dosage, initial dye concentration, and reaction time, was systematically examined. The findings revealed that Yellow 3G was more effectively degraded under acidic conditions, whereas Methylene Blue showed better removal under basic conditions. The optimal catalyst dosage for both dyes was 0.3 g/L, with optimal initial dye concentrations of 30 mg/L for Yellow 3G and 20 mg/L for Methylene Blue. The photocatalyst's stability and reusability were evaluated across five consecutive cycles. Although removal efficiency slightly decreased—from 98.23% to 82.25% for Yellow 3G and from 96.87% to 80.86% for Methylene Blue—the photocatalyst demonstrated reliable performance over repeated use. Given its high efficiency, low cost, ease of synthesis, stability, and reusability, the Fe_2O_3/Bi/GO nanocomposite offers a promising solution for the treatment of industrial wastewater and the removal of other organic pollutants.

Acknowledgments

The paper is from a PhD thesis in the Department of Environmental Engineering, Faculty of Natural Resources and Environment, University of Birjand. The authors feel it necessary to express their gratitude to the University of Birjand for its financial and moral support throughout all stages of this research.

References

Abbood, N.S., Ali, N.S., Khader, E.H., Majdi, H. S., Albayati, T.M. & Saady, N.M.C., 2023. Photocatalytic degradation of cefotaxime pharmaceutical compounds onto a modified nanocatalyst. *Research on Chemical Intermediates*, 49**,** 43-56.

Ahmadpour, N., Nowrouzi, M., Madadi Avargani, V., Sayadi, M.H. & Zendehboudi, S., 2024. Design and optimization of TiO_2-based photocatalysts for efficient removal of pharmaceutical pollutants in water: Recent developments and challenges. *Journal of Water Process Engineering*, 57**,** 104597.

Akbari, M.Z., Xu, Y., Liang, C., LU, Z., Shen, S. & Peng, L., 2023. Synthesis of ZnO@VC for enhancement of synergic photocatalytic degradation of SMX: Toxicity assessment, kinetics and transformation pathway determination. *Chemical Engineering and Processing-Process Intensification*, 193**,** 109544.

Ali, N., Said, A., Ali, F., Raziq, F., Ali, Z., Bilal, M., Reinert, L., Begum, T. & Iqbal, H.M., 2020. Photocatalytic degradation of congo red dye from aqueous environment using cobalt ferrite nanostructures: development, characterization, and photocatalytic performance. *Water, Air, & Soil Pollution*, 231**,** 1-16.

Campos-Delgado, J. & Mendoza, M.E., 2023. Ternary graphene oxide and titania nanoparticles-based nanocomposites for dye photocatalytic degradation: A Review. *Materials,* 17**,** 135.

Chang, S.-K., Abbasi, Z., Khushbakht, F., Ullah, I., Rehman, F.U. & Hafeez, M., 2024. Rapid pH-dependent photocatalytic degradation of methylene blue by CdS nanorods synthesized through hydrothermal process. *Arabian Journal of Chemistry,* 17**,** 105422.

Chauhan, A. & Chauhan, P., 2014. Powder XRD technique and its applications in science and technology. *Journal Anal Bioanal Tech,* 5**,** 1-5.

Daoush, W.M., 2017. Co-precipitation and magnetic properties of magnetite nanoparticles for potential biomedical applications. *Journal Nanomed Research,* 5**,** 00118.

Devi, S., Chahal, S., Singh, S., Kumar, P., Kumar, S., Kumar, A. & Kumar, V., 2023. Magnetic Fe_2O_3/CNT nanocomposites: characterization and photocatalytic application towards the degradation of Rose Bengal dye. *Ceramics International,* 49**,** 20071-20079.

Foroughipour, M. & Nezamzadeh-Ejhieh, A., 2023. $CaTiO_3$/g-C_3N_4 heterojunction-based composite photocatalyst: part I: experimental design, kinetics, and scavenging agents' effects in photocatalytic degradation of gemifloxacin. *Chemosphere,* 334**,** 139019.

Guo, R.-T., Wang, J., Bi, Z.-X., Chen, X., Hu, X. & Pan, W.-G., 2022. Recent advances and perspectives of g–C3N4–based materials for photocatalytic dyes degradation. *Chemosphere,* 295**,** 133834.

Hajiani, M., Sayadi, M.H., Mozafarjalali, M. & Ahmadpour, N., 2023. Green synthesis of recyclable, cost-effective, chemically stable, and environmentally friendly CuS@ Fe3O4 nanoparticles for the photocatalytic degradation of dye. *Journal of Cluster Science,* 34**,** 1939-1951.

Hajipour, F., Asad, S., Amoozegar, M.A., Javidparvar, A.A., Tang, J., Zhong, H. & Khajeh, K., 2021. Developing a fluorescent hybrid nanobiosensor based on quantum dots and azoreductase enzyme for methyl red monitoring. *Iranian Biomedical Journal,* 25**,** 8.

Huang-Mu, L., Devanesan, S., Farhat, K., Kim, W. & Sivarasan, G., 2023. Improving the efficiency of metal ions doped Fe_2O_3 nanoparticles: photocatalyst for removal of organic dye from aqueous media. *Chemosphere,* 337**,** 139229.

Kalaycıoğlu, Z., Özuğur Uysal, B., Pekcan, O.N. & Erim, F.B., 2023. Efficient photocatalytic degradation of methylene blue dye from aqueous solution with cerium oxide nanoparticles and graphene oxide-doped polyacrylamide. *ACS Omega,* 8**,** 13004-13015.

Khorasanipour, N., Iranmanesh, P., Saeednia, S. & Yazdi, S.T., 2023. Photocatalytic degradation of Naphthol Green in aqueous solution through the reusable ZnS/MoS_2/Fe_3O_4 magnetic nanocomposite. *Surfaces and Interfaces,* 36**,** 102613.

Khosravi Mohammad Soltan, F., Hajiani, M. & Haji, A., 2021. Nylon-6/poly (propylene imine) dendrimer hybrid nanofibers: An effective adsorbent for the removal of anionic dyes. *The Journal of The Textile Institute,* 112**,** 444-454.

Kumari, H., Sonia, Suman, Ranga, R., Chahal, S., Devi, S., Sharma, S., Kumar, S., Kumar, P. & Kumar, S., 2023. A review on photocatalysis used for wastewater treatment: dye degradation. *Water, Air, & Soil Pollution,* 234**,** 349.

Lanjwani, M.F., Khuhawar, M.Y., Khuhawar, T.M.J., Lanjwani, A.H., Memon, S.Q., Soomro, W.A. & Rind, I.K., 2023. Photocatalytic degradation of eriochrome black T dye by ZnO nanoparticles using multivariate factorial, kinetics and isotherm models. *Journal of Cluster Science,* 34**,** 1121-1132.

Lanjwani, M.F., Tuzen, M., Khuhawar, M.Y. & Saleh, T.A., 2024. Trends in photocatalytic degradation of organic dye pollutants using nanoparticles: a review. *Inorganic Chemistry Communications,* 159**,** 111613.

Li, Z., Undeman, E., Papa, E. & Mclachlan, M.S., 2018. High-throughput evaluation of organic contaminant removal efficiency in a wastewater treatment plant using direct injection UHPLC-Orbitrap-MS/MS. *Environmental Science: Processes & Impacts,* 20**,** 561-571.

Lotfi, S., Ouardi, M.E., Ahsaine, H.A. & Assani, A., 2024. Recent progress on the synthesis, morphology and photocatalytic dye degradation of $BiVO_4$ photocatalysts: A review. *Catalysis Reviews,* 66**,** 214-258.

Mozafarjalali, M., Hajiani, M. & Haji, A., 2020. Efficiency of Aptenia cordifolia mucilage in removal of anion dyes from aqueous solution. *International Journal of New Chemistry,* 7**,** 111-124.

Munir, A., Jamal, S., Gondal, H. Y., Iqbal, J., Hussain, A., Aziz, A., Nisar, M., Zubair, M., Momin, A. & Haider, A., 2024. Bismuth sensitized iron oxide on exfoliated graphene oxide (Bi–Fe_2O_3@ GO) for oxygen evaluation reaction. *Discover Nano,* 19**,** 193.

Naffeti, M., Zaibi, M. A., Nefzi, C., García-Arias, A.V., Chtourou, R. & Postigo, P.A., 2023. Highly efficient photodegradation of methylene blue by a composite photocatalyst of bismuth nanoparticles on silicon nanowires. *Environmental Technology & Innovation,* 30**,** 103133.

Nejati, K. & Zabihi, R., 2012. Preparation and magnetic properties of nano size nickel

ferrite particles using hydrothermal method. *Chemistry Central Journal*, 6**,** 1-6.

Poorsajadi, F., Sayadi, M. H., Hajiani, M. & Rezaei, M.R., 2021. Photocatalytic degradation of methyl orange dye using bismuth oxide nanoparticles under visible radiation. *International Journal of New Chemistry*, 8**,** 229-239.

Rafiq, A., Ikram, M., Ali, S., Niaz, F., Khan, M., Khan, Q. & Maqbool, M., 2021. Photocatalytic degradation of dyes using semiconductor photocatalysts to clean industrial water pollution. *Journal of Industrial and Engineering Chemistry*, 97**,** 111-128.

Roozbahani, P.A., Behnejad, H. & Hamzehloo, M., 2024. Synthesis, analysis, and application of zinc oxide and bismuth-based nanocomposites ($ZnO/BaBi_2O_6$) as a photocatalyst for organic dyes degradation. *Inorganic Chemistry Communications*, 168**,** 112821.

Sayadi, M.H., Ghollasimood, S., Ahmadpour, N. & Homaeigohar, S., 2022. Biosynthesis of the ZnO/SnO_2 nanoparticles and characterization of their photocatalytic potential for removal of organic water pollutants. *Journal of photochemistry and photobiology A: chemistry*, 425**,** 113662.

Sayadi, R. & Heshmatpour, F., 2024. CaAl1. 5Fe0. 5O4/6% Ni-ZnO nanocomposites: Synthesis, characterization and effective photocatalyst for the photocatalytic degradation of methylene blue dye. *Inorganic Chemistry Communications*, 169**,** 113089.

Shabil Sha, M., Anwar, H., Musthafa, F.N., Al-Lohedan, H., Alfarwati, S., Rajabathar, J. R., Khalid Alahmad, J., Cabibihan, J.-J., Karnan, M. & Kumar Sadasivuni, K., 2024. Photocatalytic degradation of organic dyes using reduced graphene oxide (rGO). *Scientific Reports*, 14**,** 3608.

Shah, R.K., 2023. Efficient photocatalytic degradation of methyl orange dye using facilely synthesized α-Fe_2O_3 nanoparticles. *Arabian Journal of Chemistry*, 16**,** 104444.

Shaikh, A.A., Patil, M.R., Jagdale, B.S. & Adole, V. A., 2023. Synthesis and characterization of Ag doped ZnO nanomaterial as an effective photocatalyst for photocatalytic degradation of Eriochrome Black T dye and antimicrobial agent. *Inorganic Chemistry Communications*, 151**,** 110570.

Singh, N., Singh, M.K., Raghuvansi, J., Yadav, R.K. & Azim, Z., 2024. Green synthesis of nano iron oxide using Emblica officinalis L. fruit extract and its impact on growth, chlorophyll content, and metabolic activity of Solanum lycopersicum L. *Journal of Applied Biology & Biotechnology*, 12**,** 173-181.

Singh, P., Hasija, A., Thakur, C., Chopra, D. & Siddiqui, K.A., 2023. Exploring the pH reliant high photocatalytic degradation of organic dyes using H-bonded Ni (II) coordination network. *Journal of Molecular Structure*, 1276**,** 134784.

Sun, H.-B., Ai, Y., Li, D., Tang, Z., Shao, Z. & Liang, Q., 2017. Bismuth iron oxide nanocomposite supported on graphene oxides as the high efficient, stable and reusable catalysts for the reduction of nitroarenes under continuous flow conditions. *Chemical Engineering Journal*, 314**,** 328-335.

Tichapondwa, S.M., Newman, J. & Kubheka, O., 2020. Effect of TiO_2 phase on the photocatalytic degradation of methylene blue dye. *Physics and Chemistry of the Earth, Parts A/B/C*, 118**,** 102900.

Tuama, A.N., Alzubaidi, L.H., Jameel, M.H., Abass, K.H., Bin Mayzan, M.Z.H. & Salman, Z. N., 2024. Impact of electron–hole recombination mechanism on the photocatalytic performance of ZnO in water treatment: A review. *Journal of Sol-Gel Science and Technology***,** 1-15.

Verma, S., Rao, B.T., Singh, R. & Kaul, R., 2021. Photocatalytic degradation kinetics of cationic and anionic dyes using Au–ZnO nanorods: Role of pH for selective and simultaneous degradation of binary dye mixtures. *Ceramics International*, 47**,** 34751-34764.

Wang, Q., Zhao, Y., Zhang, Z., Liao, S., Deng, Y., Wang, X., Ye, Q. & Wang, K., 2023. Hydrothermal preparation of Sn_3O_4/TiO_2 nanotube arrays as effective photocatalysts for boosting photocatalytic dye degradation and hydrogen production. *Ceramics International*, 49**,** 5977-5985.

Xu, Z., Zada, N., Habib, F., Ullah, H., Hussain, K., Ullah, N., Bibi, M., Bibi, M., Ghani, H. & Khan, S., 2023. Enhanced photocatalytic degradation of malachite green dye using silver–manganese oxide nanoparticles. *Molecules*, 28**,** 6241.